Available online at www.sciencedirect.com
SCIENCE DIRECT®
Thin Solid Films 449 (2004) 133–137
thin solid films
www.elsevier.com/locate/tsf

Strain-induced structural changes in thin $YBa_2Cu_3O_{7-x}$ films on $SrTiO_3$ substrates

V. Vonk[a], S.J. van Reeuwijk[a,b], J.M. Dekkers[b], S. Harkema[b], A.J.H.M. Rijnders[b], H. Graafsma[a,*]

[a]*European Synchrotron Radiation Facility, 6 rue Jules Horowitz, Grenoble 38043, France*
[b]*Low Temperature Division and MESA+Research Institute, Faculty of Science and Technology, University of Twente, P.O. Box 217, Enschede 7500 AE, The Netherlands*

Received 11 March 2003; received in revised form 29 September 2003; accepted 23 October 2003

Abstract

High-energy synchrotron radiation is used to obtain reciprocal space maps of thin $YBa_2Cu_3O_{7-x}$ films grown by pulsed laser deposition on (001) $SrTiO_3$ substrates. The films show a transition from a tetragonal to an orthorhombic structure with increasing film thickness. The critical thickness is found to be 11.5 ± 0.6 nm, whereas the thickness characterizing the tetragonal-to-orthorhombic transition is estimated to be 23 ± 1 nm. Furthermore, it is shown that for miscut angles of the vicinal substrates up to approximately 1.2°, the films grow parallel to the optical surface-normal, rather than to the crystallographic *c*-axis of the substrates. The feasibility of using high energy X-rays allows for the use of complicated sample chambers, needed for in-situ studies of the growth and behaviour of thin films under controlled atmosphere and at elevated temperatures.

Keywords: Epitaxy; Phase-transitions; Surface and interface states; X-Ray diffraction

1. Introduction

At present, thin film layered oxides such as high-T_c superconductors are of keen interest because of their applications in, e.g. electronic devices or biomagnetism. Since the interface between film and substrate determines to a great extent the structural properties and with those the physical properties of the grown film, it is of importance to study the interaction between substrate and film. In the case of *c*-axis oriented $YBa_2Cu_3O_{7-x}$ films (YBCO) on (001) $SrTiO_3$ substrates (STO), crystals of high quality can be grown using pulsed laser deposition (PLD) [1]. As known from bulk material, the superconducting properties of YBCO are highly dependent on the oxygen content, which in turn is directly related to the lattice parameters [2]. With the oxygen content changing from 6 to 7 the crystal structure changes from P4/mmm to Pmmm [3]. The additional oxygen will occupy preferentially the site in the *bc* plane, destroying the tetragonal symmetry. In fact, an oxygen content in between 6 and 7 results in different types of ordering of the oxygen and consequently different phases are formed [4] of which Ortho-I has the highest T_c around 92 K. This phase-transition as a function of oxygen content is of the so-called ferro-elastic kind, because spontaneous strain is the driving force [5]. A consequence of this ferro-elastic strain is that orthorhombic YBCO is twinned with twin walls parallel to the mutually perpendicular *hh0* and *hh0* mirror planes of the tetragonal lattice [6]. This mechanism leads to four different co-existing twin-domain orientations [7].

For orthorhombic YBCO (i.e. Ortho-I with $x\simeq0$) the bulk lattice parameters are given by $a=3.822\pm0.001$, $b=3.891\pm0.001$ and $c=11.677\pm0.002$ Å [2]. However, due to substrate-induced strain, ultra-thin films will have in-plane lattice parameters comparable to those of the substrate, which are in the case of cubic STO $a=b=3.905$ Å. Therefore the film will be tetragonal and this is the so-called pseudomorphic phase. In thicker films, i.e. around the so-called critical thickness t_c, the lattice parameters relax towards their bulk values, mainly via formation of misfit dislocations [8–10]. Therefore a tetragonal-to-orthorhombic phase transition is expected

*Corresponding author.
E-mail address: graafsma@esrf.fr (H. Graafsma).

0040-6090/04/$ - see front matter © 2003 Elsevier B.V. All rights reserved.
doi:10.1016/j.tsf.2003.10.037

to occur around t_c. The latter has already been investigated using X-ray diffraction in the case of $GdBa_2Cu_3O_{7-x}$ on STO [11]. It was found that in addition to strain release by formation of misfit dislocations also the type of growth (i.e. columnar-like) and twin-formation has to be taken into account in the total mechanism.

It is expected that since the in-plane lattice parameters of the film are changed due to substrate-induced strain, the *c*-axis of the film will be affected according to the Poisson ratio. Furthermore, the exact substrate surface-structure, together with the nucleation mechanism, will determine the epitaxial properties [12]. Méchin et al. [13] found that the *c*-axes of film and substrate are perfectly aligned, whereas Maurice et al. [14] found a misorientation in the same direction and equal to the miscut angle of the vicinal surface.

In order to gain more insight into the initial stages of the growth of YBCO thin films by PLD, it is needed to perform in-situ monitoring and subsequently modelling of the process. Recently, this has been done using surface X-ray diffraction (SXRD) for the case of deposition of STO on STO [15].

In the next section of this paper a description will be given of the sample preparation, the experimental set-up and the principles of the data treatment. Two methods will be described to characterize the structural properties of the grown films. The first uses the twinning of the samples to determine the difference in in-plane lattice parameters from either reciprocal space maps (RSM) or from ω-scans of *hhl*-type reflections. The second deals with the epitaxial properties of the film with respect to the crystallographic surface of the vicinal substrates.

2. Experimental

2.1. Sample preparation

Several thin films of different thickness were pulsed-laser deposited in a commonly used way [1]. Prior to deposition, the STO substrates were treated chemically after which they were annealed at 950 °C in flowing oxygen for 1 h such that they are single TiO_2-terminated [16]. For the ablation of the target material, which consists of a stoichiometric YBCO pellet, a KrF excimer laser is used, having a wavelength, λ, of 248 nm. The laser beam is focused using lenses, which results in a fluence of 1.3 J/cm^2. Typical deposition rates for YBCO are 1 Å/s. After deposition, the oxygen pressure is increased to approximately 0.8 bar and the sample is cooled to room-temperature with two anneal-steps, one at 600 °C and one at 450 °C both lasting 15 min. Following this procedure ensures YBCO films with the appropriate oxygen content close to 7 in a reproducible way.

2.2. Experimental set-up

All XRD experiments described herein were performed at the end-station ID15C of the high energy beamline ID15 of the European Synchrotron Radiation Facility (ESRF). This beamline consists of an asymmetric multipolewiggler (AMPW) with a critical energy of 44.1 keV, which provides the radiation for three independent end-stations. The side-station ID15C is at a fixed angle with the main beam coming from the source and a reflection of a single crystal is used to provide the monochromatic X-ray beam. This single-bounce Si(111) Laue monochromator, which can be bent elliptically to focus in the scattering plane, gives an energy of approximately 40 keV. A detailed description of the lay-out and elements of this beamline can be found elsewhere [17].

The samples are mounted on a standard Huber 511.1 diffractometer, using two sets of slits on the detector arm in order to diminish the background and obtain a high angular resolution.

Due to the similar lattice parameters of film and substrate, their diffraction peaks overlap in reciprocal space. Especially, since the *c*-axes differ about a factor of three, all the substrate reflections at the third harmonic from the monochromator overlap with film reflections at the first harmonic. Although the third harmonic is only approximately 1% of the total incoming beam intensity, the diffracting volume of the substrate is 3–4 orders larger and in addition the substrate can be considered a perfect crystal. This can lead, especially for low order reflections, to such a high signal level of the third harmonic that it saturates the detector. To circumvent this undesired effect, a multilayer consisting of 120 bilayers of WB_4C, was used to suppress higher harmonics. A detailed description about this kind of optical element can be found in Ref. [18]. The multilayer used in our set-up was constructed and characterized in the multilayer laboratory at the ESRF. The reflectivity of the first harmonic was measured to be 80% and the suppression of the third harmonic was calculated to be at least 10^3. Careful monitoring of the higher harmonics contamination, using a NaI(Tl) energy dispersive photon-counting detector, revealed no significant contribution to the measured signal.

2.3. Determination of orthorhombicity

Usually in crystallography the angular settings of several reflections of the crystal are used to refine the lattice parameters. In the case of twinned samples this method is not so straightforward, because reflections from different domains are close together in reciprocal space and centring becomes less obvious. Twinning in YBCO appears in the *hk*-plane and is visualized in Fig. 1 as four different sets of axes (a_i^*,b_i^*). The set (a_1^*,b_1^*)

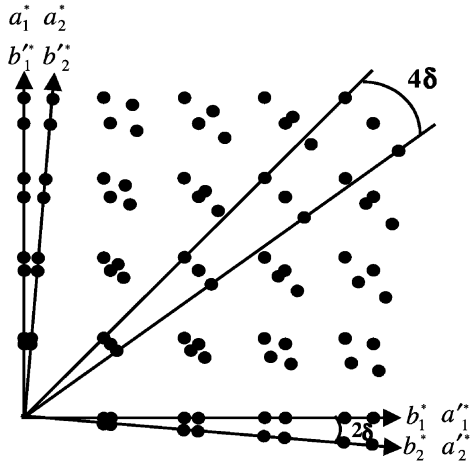

Fig. 1. Schematic overview of reciprocal space of YBCO in the $l=0$ plane. Each of the domains has corresponding axes a_i^* and b_i^* with $i=1$–2. The twinning is described by a 2δ rotation around the c*-axis and inversion of a and b axis (see text). The two outer peaks of the *hhl* reflections are separated by an angle 4δ.

is rotated over an angle 2δ with respect to the set (a_2^*,b_2^*). The other two sets are obtained by inverting the a and b axes, indicated by (b'^*_1,a'^*_1) and (b'^*_2,a'^*_2) in Fig. 1. The rotation angle 2δ is directly related to the in-plane lattice parameters by:

$$\tan\delta = \frac{b-a}{b+a} \equiv \eta \tag{1}$$

and the parameter η is the so-called orthorhombicity.

By reciprocal space mapping in the *hk*-plane of a reflection, the angle δ can be determined from the relative difference Δh and Δk between the domains. In the case of a rocking curve it depends on the position in reciprocal space where the reflection passes through the Ewald sphere. For an *hhl* reflection two of the four domains overlap (see Fig. 1), and since in this case all four domains have the same Bragg angle three peaks are seen when performing an ω-scan. For the measured angle $\Delta\omega$ between the two outer peaks the following relation holds:

$$\cos(\Delta w) = \frac{\cos(4\delta)(h^2(a^{*2}+b^{*2}))+l^2c^{*2}}{h^2(a^{*2}+b^{*2})+l^2c^{*2}} \tag{2}$$

where it is noticed that when $l=0$, the angle $\Delta\omega$ is independent of $\sin(\theta)/\lambda$. The separation of reflections, expressed in reciprocal lattice units (r.l.u.), is of course still a function of $\sin(\theta)/\lambda$. By centring on the middle peak of several *hhl* reflections an orientation matrix (OM) can be found and the lattice parameters can be refined. Using only *hhl* reflections will result in equal a and b axes, which are the average of the real orthorhombic axes, and therefore an OM of the underlying average tetragonal lattice is found. Nevertheless, the lattice parameters can then be determined from the value of η together with the average a and b from the OM.

As many reflections as possible are used to define the OM, resulting in 7 for the thinnest (7 nm) to approximately 20 for the thickest (400 nm) film. Once the OM is defined, mesh-scans of certain regions in reciprocal space can be performed. Since the splitting of the peaks is a function of $\sin(\theta)/\lambda$, high order reflections will be more suited. Here mainly the 304 and 115 reflections are used.

2.4. Determination of film orientation

In order to determine the epitaxial properties of the grown films, the orientation of the film with respect to the substrate has to be regarded. In principle, by comparison of the OM found for the film with the one of the substrate the relative orientation can be determined. However, by using the difference in angular settings of reflections of substrate and film directly, it is also possible to determine the relative orientation. In the latter case any systematic errors, like offset values of the diffractometer axes, cancel and because several reflections can be used a spread in the determined values can be calculated. Taking two reflections, one of the substrate and one of the film denoted as $\vec{H}_s$ and $\vec{H}_f$ respectively, the directions of their scattering vectors are known. For the crystal to be in diffracting position the scattering vector is aligned in the horizontal scattering plane making an angle $\frac{\pi}{2}-\theta$ with the beam. The directions of these vectors can now be written in the diffractometer-based frame by:

$$\vec{H}_f = \left(\sin\left(\frac{\pi}{2}-\theta_f\right),\cos\left(\frac{\pi}{2}-\theta_f\right),0\right) \tag{3}$$

$$\vec{H}_s = \left(\sin\left(\frac{\pi}{2}-\theta_s\right),\cos\left(\frac{\pi}{2}-\theta_s\right),0\right) \tag{4}$$

Using the angular settings of the sample on the diffractometer at these positions, denoted (ω_f, χ_f, ϕ_f) and (ω_s, χ_s, ϕ_s), it is possible to calculate the position of $\vec{H}_f$ at the angular settings of $\vec{H}_s$. This is done by first rotating $\vec{H}_f$ back to the zero position and then to the position of $\vec{H}_s$. In this way two vectors are known, both expressed in the same orthonormal lab-frame so that the angle between them can be calculated. Using the rotation matrices for a four-circle diffractometer as defined by Busing et al. [19] the required expression is given by:

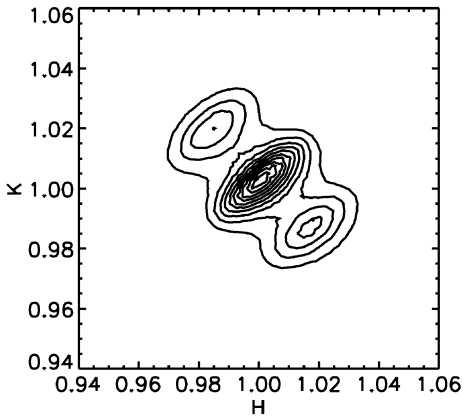

Fig. 2. An *hk*-mesh of the 115 of a 400 nm film.

$$\vec{H}_f' = R_{\omega_s,\chi_s,\phi_s} R_{-\phi_f,-\chi_f,-\omega_f} \vec{H}_f \tag{5}$$

where R is the 3×3 rotation matrix.

3. Results

Seven samples with thicknesses ranging from 7 to 400 nm were used in the measurements. Reciprocal space mapping of several *hhl* and *h0l*-type reflections is performed from which the orthorhombicity (see Eq. (1)) is determined. Fig. 2 shows an *hk*-mesh of the 115 reflection of a 400-nm film. In Fig. 3 the corresponding ω-scan of the reflection is shown. The results of the orthorhombicity of all samples are plotted in Fig. 4. The error bars have been determined by taking the spread in the calculations of the orthorhombicity from several reflections of the same sample. The thickness is estimated from the deposition parameters and therefore no error bars are indicated.

For four samples the miscut angle is determined and also the angle between the *c*-axes of film and substrate. The results are listed in Table 1. Error bars have been determined by calculating the angle using different sets of *00l* reflections for both substrate and film.

4. Discussion

Fig. 4 shows clearly a transition from tetragonal to orthorhombic with increasing film thickness. The dashed

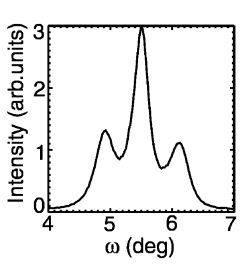

Fig. 3. An ω-scan of the 115 of a 400 nm film.

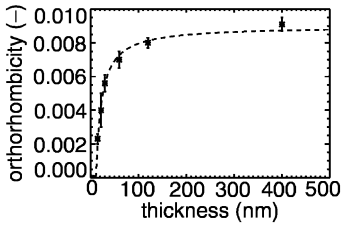

Fig. 4. Orthorhombicity η as function of film thickness. The dashed line is a fit to a $1/t$ behaviour as explained in the text.

line in Fig. 4 is obtained by a fit to all data points, except the 7 nm film, of the form:

$$\eta(t) = \eta_{max} + \frac{B}{t} \tag{6}$$

The best fit is obtained with parameters $\eta_{max} = 0.0089 \pm 0.0002$ and $B = -0.104 \pm 0.005$. The value for η_{max} corresponds very well with the reported orthorhombicity of fully oxygenated bulk YBCO with $\eta_{bulk} = 0.0089 \pm 0.0003$, calculated from Cava et al. [2]. The midway point of the transition, i.e. for $\eta = \eta_{max}/2$ corresponds to a thickness of $t_{OT} = 23 \pm 1$ nm, where the subscript OT denotes the orthorhombic-to-tetragonal transition. The fit gives a critical thickness t_c, where $\eta = 0$, of 11.5 ± 0.6 nm, which compares well with reported values in the literature for the critical thickness of YBCO on STO ranging from 8 to 13 nm [11,20,21].

The orthorhombicity for a thin film of 30 nm reported here is around $\eta = 0.005$. When taking the bulk data of Cava et al. [2] this would correspond to a T_c of 40 K and an accompanying oxygen content with $x \simeq 0.5$. However, T_c measurements on thin YBCO films by Zhai et al. [22] reveal for a 30 nm film a T_c of approximately 88 K, which relates to an oxygen content with $x \simeq 0.1$ and an orthorhombicity of 0.009. This could indicate that the STO substrate strains the YBCO film, thereby lowering the orthorhombicity without affecting the oxygen content nor the ordering of oxygen, where the latter is believed to be the fingerprint of the superconducting phase [4].

Comparing the miscut angles with the relative orientation of the film with respect to the substrate it is shown in Table 1 that up to a miscut angle of 1.2°, the film has grown on the optical rather than the crystallographic surface of the substrate. It is to be noted that

Table 1
Miscut angle and angle ξ between *c*-axes of film and substrate

Sample (nm)	Miscut (deg)	ξ (deg)	$\sigma(\xi)$ (deg)
120	0.49	0.49	–
60	0.68	0.71	0.05
30	0.69	0.61	0.07
15	1.2	0.8	0.3

the standard deviation in the measurements on the 1.2° miscut sample is relatively high. Measurements by Maurice et al. [14] on a 200 nm YBCO film on a 0.53° miscut (001) STO substrate, shows the same behaviour. Méchin et al. used vicinal (001) STO substrates with miscut angles of 2, 4 and 6° and found that YBCO films grow on the crystallographic surfaces of these substrates. This could mean that the epitaxial relationship between film and substrate is influenced by the magnitude of the miscut angle.

5. Conclusion

It is shown that YBCO films undergo structural changes as function of thickness when grown on STO and that these structural changes can be measured using high energy XRD. Due to substrate-induced strain YBCO films thinner than 11.5 ± 0.6 nm are tetragonal, whereas above this critical thickness they gradually evolve towards the bulk orthorhombicity of fully oxygenated YBCO. The thickness characteristic for this transition is 23 ± 1 nm.

Furthermore it is shown that thin YBCO films grow on the optical surface of the vicinal STO substrates up to a miscut angle of approximately 1.2°.

In order to obtain more information about the mechanisms of the structural changes in YBCO films grown on STO, experiments have to be carried out at deposition conditions, i.e. high temperatures and specific oxygen atmospheres. The use of high energy X-rays opens the possibilities for in-situ studies of the structure, because the use of complicated sample chambers is facilitated.

Acknowledgments

The authors would like to thank H.J. Smilde for the deposition of some of the thin films.

References

[1] D.B. Chrisey, G.K. Hubler, Pulsed Laser Deposition of Thin Films, John Wiley and Sons, New York, 1994.
[2] R.J. Cava, B. Batlogg, C.H. Chen, E.A. Rietman, S.M. Zahurak, D. Werder, Phys. Rev. B 36 (1987) 5719.
[3] J.D. Jorgenson, M.A. Beno, D.G. Hinks, L. Soderholm, K.J. Volin, R.L. Hitterman, J.D. Grace, I.K. Schuller, Phys. Rev. B 36 (1987) 3608.
[4] H.F. Poulsen, N.H. Andersen, J.V. Andersen, H. Bohr, O.G. Mouritsen, Nature 349 (1991) 321.
[5] J. Sapriel, Phys. Rev. B 12 (1975) 5128.
[6] F. Sandiumenge, C. Dubs, P. Görnert, S. Galí, J. Appl. Phys. 75 (1994) 5243.
[7] G.J. McIntyre, A. Renault, G. Collin, Phys. Rev. B 37 (1988) 5148.
[8] J.P. Contour, A. Défossez, D. Ravelosona, A. Abert, P. Ziemann, Z. Phys. B 100 (1996) 185–190.
[9] S.K. Streiffer, B.M. Lairson, C.B. Eom, B.M. Clemens, J.C. Bravman, Phys. Rev. B 43 (1991) 13 007.
[10] A. Del Vecchio, M.F. De Riccardis, L. Tapfer, J. Vac. Sci. Technol. A 18(3) 802.
[11] L.X. Cao, T.L. Lee, F. Renner, Y.X. Su, R.L. Johnson, J. Zegenhagen, Phys. Rev. B 65 (2002) 113 402.
[12] T. Haage, J. Zegenhagen, H.-U. Habermaier, M. Cardona, Phys. Rev. Lett. 80 (1998) 4225.
[13] L. Méchin, P. Berghuis, J.E. Evetts, Physica C 302 (1998) 102–112.
[14] J.-L. Maurice, O. Durand, M. Drouet, J.-P. Contour, Thin Solid Films 319 (1998) 211–214.
[15] G. Eres, J.Z. Tischler, M. Yoon, B.C. Larson, C.M. Rouleau, D.H. Lowndes, P. Zschack, Appl. Phys. Lett. 80 (2002) 3379.
[16] G. Koster, B.L. Kropman, A.J.H.M. Rijnders, D.H.A. Blank, H. Rogalla, Appl. Phys. Lett. 73 (1998) 2920.
[17] Th. Tschentscher, P. Suortti, J. Synchrotron Radiat. 5 (1998) 286–292.
[18] D.H. Bilderback, B.M. Lairson, T.W. Barbee, G.E. Ice, C.J. Sparks, Nucl. Instrum. Methods 208 (1983) 251.
[19] W.R. Busing, H.A. Levy, Acta Cryst. 22 (1967) 457–464.
[20] K. Kamigaki, H. Terauchi, T. Terashima, K. Yamamoto, K. Hirata, K. Hayashi, I. Nakagawa, Y. Tomii, J. Appl. Phys. 69 (1991) 3653.
[21] J. Zegenhagen, T. Siegrist, E. Fontes, L.E. Berman, J.R. Patel, Solid State Commun. 98 (1995) 763.
[22] H.Y. Zhai, W.K. Chu, Appl. Phys. Lett. 76 (2000) 3469.